Published in final edited form as:
Biochemistry. 2012 April 3; 51(13): 2930–2939. doi:10.1021/bi3000879.

Aldehyde Oxidase Functions as a Superoxide Generating NADH Oxidase: An Important Redox Regulated Pathway of Cellular Oxygen Radical Formation

Tapan K. Kundu, **Murugesan Velayutham**, and **Jay L. Zweier***
Center for Biomedical EPR Spectroscopy and Imaging, the Davis Heart and Lung Research Institute, and Division of Cardiovascular Medicine, Department of Internal Medicine, The Ohio State University College of Medicine, Columbus, OH 43210, USA

Abstract

The enzyme aldehyde oxidase (AO) is a member of the molybdenum hydroxylase family that includes xanthine oxidoreductase (XOR); however, its physiological substrates and functions remain unclear. Moreover, little is known about its role in cellular redox stress. Utilizing electron paramagnetic resonance spin trapping we measured the role of AO in the generation of reactive oxygen species (ROS) through the oxidation of NADH, and the effects of inhibitors of AO on NADH-mediated superoxide ($O_2^{\bullet -}$) generation. NADH was found to be a good substrate for AO with apparent K_m and V_{max} values of 29μM and 12 nmol min^{-1} mg^{-1}, respectively. From $O_2^{\bullet -}$ generation measurements by cytochrome c reduction the apparent K_m and V_{max} values of NADH for AO were 11 μM and 15 nmol min^{-1} mg^{-1}, respectively. With NADH oxidation by AO, ≥65% of the total electron flux led to $O_2^{\bullet -}$ generation. Diphenyleneiodonium completely inhibited AO-mediated $O_2^{\bullet -}$ production confirming that this occurs at the FAD site. Inhibitors of this NADH-derived $O_2^{\bullet -}$ generation were studied with amidone the most potent exerting complete inhibition at 100 μM concentration, while 150 μM menadione, raloxifene or β-estradiol led to 81%, 46% or 26% inhibition, respectively. From the kinetic data, the levels of AO and NADH, $O_2^{\bullet -}$ production was estimated to be ~89 and ~4 nM/s in liver and heart, respectively, much higher than that estimated for XOR under similar conditions. Owing to the ubiquitous distribution of NADH, aldehydes, and other endogenous AO substrates, AO is predicted to have an important role in cellular redox stress and related disease pathogenesis.

Keywords

aldehyde oxidase; superoxide; NADH; ROS; free radical; molybdenum hydroxylases; EPR; spin trapping; xanthine oxidoreductase; ischemia

Aldehyde oxidase[1] (AO; EC 1.2.3.1) is a cytosolic enzyme and belongs to the molybdenum hydroxylase family along with xanthine dehydrogenase (XDH; EC 1.1.1.204) and xanthine oxidase (XO; EC 1.1.3.22), collectively known as xanthine oxidoreductase (XOR). In their

*Corresponding author: Davis Heart and Lung Research Institute, 473 W 12th Avenue, Suite 611, The Ohio State University, Columbus, OH 43210. Jay.Zweier@osumc.edu; Tel: (614) 247-7788; Fax: (614) 247-7845.

[1]***Abbreviations used:*** AO, aldehyde oxidase; DEPMPO, 5-(diethoxyphosphoryl)-5-methyl-1-pyrroline-*N*-oxide; DPI, diphenyleneiodonium chloride; DTPA, diethylenetriaminepentaacetic acid; EDTA, ethylenediaminetetraacetic acid; EPR, electron paramagnetic resonance; FAD, flavin adenine dinucleotide; Moco, molybdenum cofactor; NOS, nitric oxide synthase; PAGE, polyacrylamide gel electrophoresis; *p*-DMAC, 4-(dimethylamino)cinnamaldehyde; RNS, reactive nitrogen species; ROS, reactive oxygen species; SOD1, copper-zinc superoxide dismutase; TCA, tricarboxylic acid; XDH, xanthine dehydrogenase; XO, xanthine oxidase; XOR, xanthine oxidoreductase.

catalytically active forms both AO and XOR exist as a homodimer of molecular weight ~300 kDa. Each monomer consists of three domains (Fig. 1) — an N-terminal domain (20 kDa) containing two spectroscopically distinct 2Fe-2S centers, a 40 kDa intermediate domain containing a flavin adenine dinucleotide (FAD) binding site, and a C-terminal domain (85 kDa) containing the substrate binding pocket as well as the molybdenum cofactor (Moco) binding site (1, 2).

Despite their remarkable similarities in cofactor composition, amino acid sequence, molecular mass, primary and secondary structures, and common genetic origin, XOR and AO have different substrate and inhibitor specificities. AO catalyzes the oxidative hydroxylation of a wide variety of substrates including a number of aliphatic and aromatic aldehydes, nitrogen containing heterocyclic compounds, and certain drugs of pharmacological interest (3–5). Moreover, under anaerobic conditions AO can catalyze the nitroreduction of environmental pollutants such as 2-nitrofluorene, 1-nitropyrene, and 4-nitrobiphenyl (6). On the other hand, XOR is mainly involved in the catabolism of purines, pyrimidines, hypoxanthine, and xanthine. Thus, compared to XOR, the active site or substrate binding pocket of AO appears to be relatively large with more flexibility as it can accommodate a diverse range of substrates.

Tissue distribution and levels of AO are markedly different from that of XOR. For example, in mammals, liver is by far the richest source of AO, followed by lung, spleen, brain, heart, testis, and eye (7, 8). On the other hand, XOR is highly expressed in the small intestine, liver, and lactating mammary gland, with lower levels in lung, heart, and other tissues (9–11). Thus, AO and XOR are predicted to have different tissue-specific biological functions.

Under normal physiological conditions more than 80% of total XOR exists as XDH (12, 13) that preferentially transfers its electrons to NAD^+ producing NADH. However, under pathological conditions XDH is believed to be converted into XO which produces superoxide ($O_2^{\bullet-}$) and hydrogen peroxide (H_2O_2) by transferring its electrons to molecular oxygen (O_2). Cysteine residues responsible for the conversion of XDH to XO have been identified as Cys^{535} and Cys^{992} that are well conserved in all mammalian XDH (14). However, in AO these residues are replaced by tyrosine residues (15) and therefore, conversion of AO to its dehydrogenase form does not occur. While in their FAD domain all mammalian XOR proteins are endowed with a particular tyrosine residue responsible for the binding of NAD^+, AO is devoid of this tyrosine residue (16). Thus, unlike XOR, AO does not require the NAD^+ cofactor for its catalytic activity, rather it exists as a permanent oxidase and exclusively transfers its electrons to O_2 with concomitant production of $O_2^{\bullet-}$ and H_2O_2.

Owing to its ability to generate reactive oxygen species (ROS), such as $O_2^{\bullet-}$ and H_2O_2, and its suggested role in reperfusion injury (17) and cardiovascular diseases (18), XOR has been the subject of intense investigation over the past 25 years. On the other hand, although AO is known for its role in the metabolism of certain drugs and detoxification of xenobiotics, there has been little investigation regarding its endogenous substrates, physiological functions, and role in oxidant biology. Recently, we have shown that compared to XO in the presence of optimal xanthine level, AO in the presence of aldehyde substrate can produce higher amounts of $O_2^{\bullet-}$ (19). We have also shown that AO is a key enzyme in the generation of nitric oxide (NO) from nitrite reduction during ischemia and the amount of NO produced is of comparable magnitude to that produced by constitutive nitric oxide synthase (NOS) (20, 21). Thus, in addition to the metabolism of drugs, AO could serve as an important biological source of ROS, NO, and reactive nitrogen species (RNS) and may play a vital role in ROS- or RNS-mediated signaling and tissue injury.

In addition to aldehydes, NADH can also serve as a substrate for $O_2^{\bullet-}$ formation by AO; however, there is a lack of knowledge regarding the kinetics and the magnitude of $O_2^{\bullet-}$ production that occurs. By utilizing electron paramagnetic resonance (EPR) spin trapping techniques and the cytochrome c reduction assay, we characterize the process of NADH-mediated $O_2^{\bullet-}$ production by AO and the effect of various inhibitors of AO on this process. Given the levels of AO and its enzymatic activity, as well as the concentrations of NADH in biological tissues, it is evident that AO functions as a source of both $O_2^{\bullet-}$ and H_2O_2 under normal physiological conditions with an important role in cellular redox stress and related disease.

Materials and Methods

Materials

Ethylenediaminetetraacetic acid (EDTA) disodium salt, phenylmethanesulfonyl fluoride (PMSF), 4-(Dimethylamino)cinnamaldehyde (*p*-DMAC), xanthine, potassium phosphate (both dibasic and monobasic salts), sodium chloride, sodium hydroxide, sodium pyrophosphate, cytochrome c from horse heart, catalase, copper-zinc superoxide dismutase (SOD1), xanthine oxidase, menadione, β-estradiol, raloxifene, methanol, acetonitrile, dimethyl sulfoxide (DMSO), and HR Sephacryl S-300 were purchased from Sigma. Bovine serum albumin (BSA), protein determination kit, 4–15% precast gel, sample buffers, β-mercaptoethanol, and chromatographic columns were obtained from Bio-Rad. Benzamidine Sepharose 6B, Sephadex G-25, and molecular weight marker for native gel were obtained from GE-Healthcare Bio-Sciences. BioSepra Hydroxyapatite Ultrogel was purchased from Paal Life Sciences, PA. Diphenyleneiodonium chloride (DPI) was purchased from Cayman Chemical and amidone from Xanodyne Pharmaceuticals Inc., Newport, KY. Diethylenetriaminepentaacetic acid (DTPA) was purchased from Aldrich. Spin trapping agent, 5-(diethoxyphosphoryl)-5-methyl-1-pyrroline-*N*-oxide (DEPMPO) was purchased from Alexis (Carlsbad, CA). All other chemicals used in this study were of the highest quality commercially available.

Isolation and Purification of AO

Livers from male Sprague-Dawley rats (250–300 g) were excised and the residual blood was removed by rinsing thoroughly with 0.15 M phosphate buffer saline solution (pH 7.4) containing 0.9% NaCl. Livers were subsequently frozen in liquid nitrogen and stored at −80 °C until needed. Purifications of AO from these frozen livers were performed at 2–3 °C according to our prior reported protocol (19). Briefly, the liver cytosol was prepared from the homogenate by centrifuging, followed by heat-treatment and ammonium sulfate fractionation. This cytosolic extract was then chromatographed on a Hydroxyapatite Ultrogel column and the protein was eluted with phosphate buffer. The concentrated protein was then chromatographed on a HR Sephacryl S-300 gel filtration column and after eluting the protein it was further purified by affinity chromatography on a Benzamidine Sepharose 6B column.

Native polyacrylamide gel electrophoresis

Electrophoresis was performed on a pre-cast gradient gel (4–15%) using a constant current of 5 mA for 14 hours at 3 °C. Standard native molecular weight marker (66–669 kDa) was used. Finally the gel was stained with 0.25% Coomassie brilliant blue R-250 and destained with a solution containing 15% methanol and 10% acetic acid (19). All buffers used were devoid of any SDS or other reducing agents.

Assays for enzyme activity and determination of protein concentration

Activity of AO was determined spectrophotometrically by using *p*-DMAC as a substrate and O_2 as an electron acceptor. The reaction mixture, in a final volume of 1 mL, consisting of 25 μM *p*-DMAC in air-saturated potassium phosphate buffer (50 mM, pH 7.8) containing 0.1 mM EDTA was incubated in a quartz cuvette of 1 cm path length. A catalytic amount of enzyme solution was added to initiate the reaction and the oxidation of the substrate was followed immediately by monitoring the decrease in absorbance at 398 nm. All the measurements were carried out on Cary-50 UV-Vis spectrophotometer equipped with a thermostated cell compartment. Absorbance changes were converted to units of enzyme activity (IU) using an extinction coefficient of 30,500 M^{-1} cm^{-1} (22). One unit of enzyme activity is defined as the amount of enzyme required to oxidize one micromole of *p*-DMAC per minute at 30 °C.

Similarly, the activity of XO was determined by using the same buffer, but the reaction mixture contained 30 μM of xanthine as substrate. A suitable volume of enzyme solution was added to initiate the oxidation of xanthine and the formation of uric acid was monitored by following the increase in absorbance at 295 nm. The activity of the enzyme was calculated from the absorbance changes by using an extinction coefficient of 6,780 M^{-1} cm^{-1} (23).

Protein concentration was determined by the Bradford method (24), using Bio-Rad protein assay kit and bovine serum albumin as a standard.

Electron paramagnetic resonance spectroscopy

The X-band electron paramagnetic resonance (EPR) spectra were recorded on a Bruker ESP 300E spectrometer equipped with a TM_{110} microwave cavity. The instrument was also equipped with a proton probe gaussmeter and a microwave frequency counter to enable precise calibration of magnetic field and microwave frequency as described previously (25). EPR measurements were performed at ambient temperature using the spin trap DEPMPO with placement of the reaction mixture in a quartz EPR flat cell. The EPR instrument parameters were chosen to optimize sensitivity (26–28) and were as follows: microwave frequency, 9.78 GHz; microwave power, 20 mW; modulation amplitude, 0.5 (for figure 2 only) or 1 G; time constant, 40 (for figure 2 only) or 82 ms; scan time, 1 min.

Kinetics of NADH oxidation and superoxide radical formation

All the kinetic and spectral measurements were carried out on Cary-50 UV-Vis spectrophotometer. The reaction mixture (total volume 1 mL) consisting of 50 mM air-saturated potassium phosphate buffer (pH 7.8) containing 0.1 mM EDTA, 100 U/mL catalase, 250 U/mL SOD1, and variable concentrations of NADH was incubated in a quartz cuvette of path length 1 cm at 21 °C. Using the fixed amount of AO (20 mU/mL, final concentration) the concentrations of NADH were varied from 5–120 μM and in each case the oxidation of NADH was monitored at 340 nm. The initial rates were calculated by using the extinction coefficient of 6,220 M^{-1} cm^{-1} and the kinetic parameters for the substrate consumption were determined from these data by fitting them to Michaelis-Menten equation using SigmaPlot 11.0.

The original rates of $O_2^{\bullet -}$ generation were determined by monitoring the SOD1-inhibitable reduction of ferricytochrome c at 550 nm. The reaction mixture (1 mL) consisting of 100 μM ferricytochrome c, 100 mM potassium phosphate buffer (pH 7.8) containing 0.1 mM EDTA, 100 U/mL catalase, and variable concentrations of NADH was incubated in a quartz cuvette of 1 cm path length at 21 °C. The enzyme solution (29 mU/mL AO, final concentration) was added last to initiate the reaction and the absorbance change at 550 nm

was recorded. In order to measure any background $O_2^{\bullet-}$-independent change in absorbance at 550 nm assays were repeated in the presence of 250 U/mL SOD1 without adding any AO. The actual rates of $O_2^{\bullet-}$ generation were calculated by subtracting the background rates from the original rates. The velocities were calculated by using these actual rates and an extinction coefficient of 21,000 M^{-1} cm^{-1} (29) for cytochrome c (the difference between the absorption of reduced cytochrome c minus oxidized cytochrome c) and the data were then fitted to the Michaelis-Menten equation to obtain the kinetic parameters for the $O_2^{\bullet-}$ generation. Cytochrome c used in all these experiments was prepared by treatment with potassium ferricyanide and subsequent passage through a Sephadex G-25 column.

Calculation of the percentage of one electron flux

The percentage of one-electron flux during the oxidation of NADH by AO was calculated as half the ratio of rate of cytochrome c reduction and the rate of NADH oxidation in air-saturated phosphate buffer as described in the literature (30).

Statistical Analysis

Values are expressed as the mean of at least three repeated measurements and reported ± standard error (SE), unless noted otherwise. Statistical significance of difference was evaluated by the student's t-test. A *P* value of 0.05 or less was considered to indicate statistical significance.

Results

The AO was purified to homogeneity with specific activity of 1.8 U/mg similar to values reported for the highly purified enzyme (31). The purified enzyme exhibited a characteristic absorbance spectrum with A_{280}:A_{450} ratio between 5.3 and 5.7 and the purity of the enzyme was further checked with native polyacrylamide gel electrophoresis (PAGE) showing a single band at 290 kDa (data not shown) indicating that the purified AO was free from other protein impurities.

EPR Spin Trapping Studies of $O_2^{\bullet-}$ Generation by AO

EPR spin trapping provides a direct method to detect and quantitate reactive free radicals including $O_2^{\bullet-}$, hydroxyl, and other oxygen-, carbon-, or sulfur-centered radicals. In order to determine the generation of $O_2^{\bullet-}$ by AO in the presence of NADH, EPR spin trapping experiments were performed using DEPMPO as a spin trap, which forms a stable EPR-detectable $O_2^{\bullet-}$-adduct with a half-life of ~15 min. EPR spectra corresponding to DEPMPO-OOH were recorded as a function of time for 20 minutes as illustrated in Fig. 2A. Our experiments revealed that AO in the presence of NADH was a potent source of $O_2^{\bullet-}$ with maximum rate of generation during the first 5 minutes from the start of the reaction. The intensity of the EPR signal of the DEPMPO-OOH adduct rapidly increased over the first 5 minutes followed by a further gradual increase with a maximum at 22 min (Fig. 2B).

NADH Oxidation

Oxidation of NADH by AO was found to be slow but progressive and monitored at 340 nm by varying the concentration of NADH from 5–120 μM. Both catalase (100 U/mL) and SOD1 (250 U/mL) were used to avoid any inactivation of the enzyme by the reaction products. The initial velocities were plotted against the concentrations of NADH and the data were fitted to the Michaelis-Menten equation (Eq. 1) as depicted in Fig. 3 (*left*).

$$V_0 = \frac{V_{\max} \cdot [S]}{K_m + [S]} \quad \text{(Eq. 1)}$$

where V_0, V_{max}, [*S*], and K_m represent the initial velocity, maximum velocity, substrate concentration, and Michaelis constant, respectively. The Lineweaver-Burk plot of these data is shown in Fig. 3 (*right*). From the NADH-oxidase activity of AO the apparent K_m value of NADH for AO was found to be 29.1 ± 4.5 μM whereas the V_{max} value was 11.9 ± 0.7 nmol min^{-1} mg^{-1} of protein. The apparent K_m value is in good agreement with the value (28 μM) reported in the literature (32).

Detection of $O_2^{\bullet -}$ by Cytochrome c Reduction Assay

The formation of $O_2^{\bullet -}$ by AO-mediated oxidation of NADH as was detected by this assay based on the ability of $O_2^{\bullet -}$ to reduce ferricytochrome c,

$$\text{Ferricytochrome } c\,(Fe^{3+}) + O_2^{\bullet -} \rightarrow \text{Ferrocytochrome } c\,(Fe^{2+}) + O_2.$$

The original rates of cytochrome c reduction by $O_2^{\bullet -}$ were calculated in the presence of variable concentrations of NADH (5–120 μM) but with a fixed amount of AO (29 mU/mL) and catalase (100 U/mL). In order to determine the actual rates, a set of control experiments in the presence of SOD1 (without adding any AO) were carried out. The rates of these control experiments were subtracted from the original rates so as to obtain the actual rates of cytochrome c reduction by AO-generated $O_2^{\bullet -}$. The initial velocities were plotted against the concentrations of NADH and the data were fitted to the Michaelis-Menten equation (Fig. 4 (*left*)). The Lineweaver-Burk plot of these data is shown in Fig. 4 (*right*). From the cytochrome c reduction by AO-mediated $O_2^{\bullet -}$, the apparent K_m and V_{max} values of NADH for AO were calculated as 10.7 ± 0.9 μM and 14.8 ± 0.4 nmol min^{-1} mg^{-1} of AO, respectively.

As the oxidation of NADH by AO produces both $O_2^{\bullet -}$ and H_2O_2, the percentage of one-electron flux can be calculated (30) from the rates of cytochrome c reduction and the oxidation of NADH as described below (Eq. 2):

$$\text{One} - \text{electron flux}\,(\%) = \frac{\text{Rate of cytochrome } c \text{ reduction}}{\text{Rate of NADH oxidation}} \times 50 \quad \text{(Eq. 2)}$$

The percentage of one-electron flux has been found to be dependent on the concentration of NADH and it decreases with increasing the concentration of NADH (Fig. 5). From this it is evident that more than 65% of the electrons released from the oxidation of NADH (100 μM) by AO lead to the formation of $O_2^{\bullet -}$. Of note, with lower NADH levels the percent of one electron flux increases with over 80 % $O_2^{\bullet -}$ production when NADH levels are less than 25 μM, and over 90% when NADH levels are below 12 μM. While the percentage of one-electron flux increases as the concentration of NADH decreases, the rate of NADH oxidation or cytochrome c reduction increases with increasing the NADH concentration and therefore, fit to Michaelis-Menten equation was not significantly affected (Figs. 3 and 4).

In order to quantitate the amount of $O_2^{\bullet -}$ formed from the oxidation of NADH by AO, we performed the cytochrome c reduction assay in the presence of 120 μM NADH and 22 mU/mL of AO (Fig. 6A, a). To further confirm that the observed reduction is due to only AO-

generated $O_2^{\bullet-}$, we performed similar experiments in the presence of SOD1 (Fig. 6A, b) as well as in the absence of AO (Fig. 6A, c). In either case there was no reduction of cytochrome c, as in the first case SOD1 completely quenched the $O_2^{\bullet-}$ and in the second case no $O_2^{\bullet-}$ was generated without AO. We also carried out an additional experiment with amidone, a potent inhibitor of AO (Fig. 6A, d) in which no $O_2^{\bullet-}$ production was observed due to the complete inhibition of AO by amidone. Therefore, it is quite clear from this study that the $O_2^{\bullet-}$ generated during the oxidation of NADH by AO is responsible for the reduction of cytochrome c. The amount of $O_2^{\bullet-}$ formed due to the oxidation of NADH by AO was found to be 19.2 ± 1.5 nmol min^{-1} mg^{-1} of AO (Fig. 6B). NAD^+ has no effect on the rate of $O_2^{\bullet-}$ production by AO and NADH as the rate remained unchanged in the presence of 500 μM NAD^+ (*data not shown*). Lack of any effect of NAD^+ on the rate of $O_2^{\bullet-}$ generation by AO is consistent with its lack of NAD^+ binding site (16).

Effects of Inhibitors of AO on the Generation of $O_2^{\bullet-}$

To further confirm the $O_2^{\bullet-}$ generation by AO and NADH as well as to characterize the effects of various inhibitors on this, parallel EPR experiments were carried out using different AO-inhibitors whose chemical structures are depicted in Fig. 7. While the inhibition of AO by menadione and β-estradiol are mixed types, though predominantly uncompetitive in nature (33), the inhibition by raloxifene is completely uncompetitive (34). Amidone exhibits a mixed non-competitive type of inhibition of AO (35). The reaction mixture containing DEPMPO (20 mM), and NADH (120 μM) was incubated in air-saturated phosphate buffer (50 mM, pH 7.8) containing 0.4 mM DTPA. As seen in Fig. 8a, no EPR signal was observed in the absence of AO. However, addition of AO (25 mU/mL) resulted in the formation of the characteristic EPR spectrum corresponding to the DEPMPO-OOH adduct (Fig. 8b) and most of the $O_2^{\bullet-}$ formation was observed during the first 10 minutes. Moreover, addition of SOD1 in the reaction mixture completely quenched the EPR signals (Fig. 8c). Addition of specific inhibitors, such as β-estradiol or raloxifene at 150 μM concentration only partially decreased the EPR signal of the DEPMPO-OOH adduct with 26% or 46% decrease seen respectively (Figs. 8d and 8e). With further 2-fold increase in the concentration of raloxifene still only 68% inhibition was seen (data not shown). In the presence of widely used AO inhibitor menadione at 150 μM concentration the DEPMPO-OOH adduct signal was largely decreased with 81% inhibition (Fig. 8f) and at 300 μM level 88% inhibition was seen (data not shown). On the other hand, amidone at 100 μM concentration almost completely (>99%) abolished the EPR signal as did DPI, a nonspecific inhibitor of FAD containing enzymes, (Figs. 8g and 8h). The effects of the various inhibitors of AO on this NADH-dependent $O_2^{\bullet-}$ generation as obtained from repeat EPR measurements are summarized in Fig. 9. Thus, it is quite evident that NADH is an effective substrate of AO capable of producing large amounts of $O_2^{\bullet-}$ and among all the inhibitors tested amidone and DPI were the most potent.

In order to examine the specificity of amidone towards the inhibition of the $O_2^{\bullet-}$ generation by AO we performed further EPR experiments with XO using NADH as a reducing substrate (Fig. 10A). It is quite evident from the strong EPR signals of DEPMPO-OOH adducts observed (Fig. 10A, a) that AO produces a large amount of $O_2^{\bullet-}$ with utilization of NADH as reducing substrate. The EPR signals corresponding to DEPMPO-OOH adduct were almost completely quenched (Fig. 10A, b) by amidone (100 μM). Moreover, amidone fully inhibited AO-mediated $O_2^{\bullet-}$ generation when *p*-DMAC (that binds to the molybdenum site) was used as a substrate (data not shown). If amidone was bound at the molybdenum site, $O_2^{\bullet-}$ generation would have still been seen with NADH as substrate. Since amidone fully inhibited $O_2^{\bullet-}$ generation from NADH, it is clear that it inhibits AO by binding to its

FAD site thereby shuting off the electron flow from this site to O_2. With NADH as substrate for XO the EPR signals corresponding to DEPMPO-OOH adducts are clearly much less, about 35% those from similar enzyme levels of AO (Fig. 10A, c) and no decrease is seen in the presence of 100 μM amidone (Fig. 10A, d) or even upon increasing the amidone concentration up to 1 mM (Fig. 10A, e). The corresponding EPR signal intensities from a series of measurements are shown in Fig. 10B. Similar results were observed when specific substrates were used that bind to the molybdenum site, *i.e., p*-DMAC for AO and xanthine for XO (data not shown). This study clearly demonstrates that compared to XO, AO produces more $O_2^{\bullet-}$. While amidone is found to be a potent inhibitor of $O_2^{\bullet-}$ production by AO, it does not exert any inhibition of XO.

Discussion

Role of AO in drug metabolism is well documented as it can metabolize a number of pharmacologically important drugs including the cardiac stimulant carbazeran, the antimalarial agent quinine, the antipsychotic agent ziprasidone, the antiviral agent famciclovir, and certain cancer-chemotherapeutic agents such as methotrexate and 6-methylthiopurine (5, 36, 37). However, little information is available on the physiological functions of AO and its endogenous substrates. Its role in the generation of ROS and related redox signaling or oxidative injury remains unclear.

NADH is found in all living cells and serve as the critical source of electrons for mitochondrial electron transport with ATP synthesis. The NAD^+/NADH balance in tissues is regulated by the tissue perfusion supporting glycolytic and tricarboxylic acid (TCA) cycle-mediated NADH production as well as the process of its utilization by the mitochondria for aerobic metabolism. While most prior reports on the function of AO have focused on aldehyde substrates, we observe that NADH also functions as an effective source of reducing equivalents triggering $O_2^{\bullet-}$ production from the enzyme. The cytochrome c reduction assays provide proof of $O_2^{\bullet-}$ generation by AO using NADH as a reducing substrate as this reduction is completely quenched by SOD1 which dismutates the $O_2^{\bullet-}$ at a rate much faster (10^3 times) than the rate of reduction of cytochrome c by $O_2^{\bullet-}$ (Fig. 6A, B). The potent AO inhibitor amidone totally quenched this cytochrome c reduction (Fig. 6A, B). Further definitive proof of $O_2^{\bullet-}$ production was provided by EPR spin trapping studies. The prominent EPR spectrum characteristic of the $O_2^{\bullet-}$-spin-adducts of DEPMPO (*i.e.* DEPMPO-OOH) was seen (Fig. 2A). As the EPR signals were not observable in the absence of AO and were completely quenched by SOD1 or inhibited by various inhibitors of AO (Fig. 8), it is quite clear that AO produces $O_2^{\bullet-}$ during the oxidation of NADH.

Surprisingly, raloxifene, a specific and potent inhibitor of human liver AO, and β-estradiol showed only weak inhibition whereas menadione, amidone and DPI exhibited potent inhibition (Fig. 9). The EPR signals corresponding to DEPMPO-OOH adduct generated during the oxidation of NADH by AO in the presence of DEPMPO were completely quenched in the presence of amidone (Fig. 10A, b). However, the similar EPR signals when generated by NADH/XO were unaffected even in the presence of 10-fold higher amidone levels (Figs. 10A, e and 10B, e). Thus, amidone serves as a potent and specific inhibitor of AO and it binds to the FAD site of the enzyme blocking NADH driven $O_2^{\bullet-}$ generation from this site, similar to menadione, β-estradiol, and DPI.

While XO has been widely recognized as an important source of ROS formation and redox stress, in human liver the activity of AO (22.4 mU/mg) (38) is reported to be 24-fold higher than that of XO (0.9 mU/mg) (23). The levels of these molybdenum hydroxylases in liver are much higher than in hearts (Table 1). While the levels of AO and total XOR in rat livers

and hearts are similar, the activities of AO are higher than those of XOR and much higher than XO (11-fold higher in liver and 25-fold higher in heart for AO compared to XO). Therefore, AO would be expected to predominate over XO as a major cytosolic source of ROS and play an important role in redox signaling processes as well as in ROS-mediated cellular and tissue injury/death.

In addition to the relative enzyme activities of XO and XDH compared to AO, it is important to characterize the one electron reduction of oxygen leading to $O_2^{\bullet-}$ production. Analysis of the steady-state kinetic parameters of NADH oxidation (K_m = 29.1 μM and V_{max} = 11.9 nmol min^{-1} mg^{-1} of protein) and $O_2^{\bullet-}$ generation (K_m = 10.7 M and V_{max} = 14.8 nmol min^{-1} mg^{-1} of protein) by AO indicates that the K_m values are below the tissue levels of NADH in normal liver and heart (Table 2). The K_m values of NADH oxidation and $O_2^{\bullet-}$ production are not necessarily the same and a two- to three-fold variation for human milk XDH has been observed (39). While the K_m value for NADH oxidation reported here is very close to the literature value (28 M) (32), the K_m value for $O_2^{\bullet-}$ generation is found to be twice the value (5.1 μM) reported recently (40); however, our V_{max} value is higher. This discrepancy may be attributed to the different buffer solutions, enzyme conditions, and assays used. The percentage of $O_2^{\bullet-}$ flux during the oxidation of NADH by rat liver XOR was reported to be almost constant (45–50%) and independent of the concentration of NADH (40). However, the kinetic parameters for the oxidation of NADH by bovine milk XO could not be determined as it deviated from the saturation kinetics. Only 37% of $O_2^{\bullet-}$ was shown to be produced during NADH oxidation by bovine milk XO (41), whereas under similar assay conditions oxidation of 100 μM NADH by AO generates about 65% $O_2^{\bullet-}$ and this value increases to > 80% when NADH levels are less than 25 μM (Fig. 5). Thus, AO-catalyzed oxidation of NADH produces much more $O_2^{\bullet-}$ than when catalyzed by either rat liver XOR or bovine milk XO. Moreover, unlike rat liver XOR, the percentage of $O_2^{\bullet-}$ formation from AO increases with decreasing concentrations of NADH, indicating more $O_2^{\bullet-}$ generation even at normal physiological conditions when the levels of NADH are very low. This is mainly because of the fact that when the substrate concentration is below its K_m value the enzyme exists mostly in 2-electron reduced form and during turn-over the reduced enzyme transfers one electron at a time to produce two molecules of $O_2^{\bullet-}$. However, at higher substrate concentration when the enzyme is mostly in the 4-electron reduced form both $O_2^{\bullet-}$ and H_2O_2 are formed as the reduced enzyme first rapidly transfers two electrons to produce one molecule of H_2O_2 and subsequently one electron at a time generating two molecules of $O_2^{\bullet-}$. Therefore, AO-mediated NADH oxidation could serve as an important pathway of $O_2^{\bullet-}$ generation in tissues even under normal physiological conditions and may be involved in cellular oxidant-mediated signaling.

From the kinetic data presented here, the measured levels of AO and the known levels of NADH in the liver and heart, it is possible to estimate the $O_2^{\bullet-}$ generation by AO-catalyzed oxidation of NADH in these tissues. In the presence of physiological levels of NADH (100 μM) the AO-mediated $O_2^{\bullet-}$ production would be 89 nM/s in liver and 4 nM/s in heart. These values are much higher than those estimated for XO-catalyzed oxidation of NADH. Due to higher catalytic turnover these values would be expected to be even higher when a reducing substrate that binds to the molybdenum site is present. Therefore, NADH-mediated $O_2^{\bullet-}$ generation by AO can play a major role under various physiological and pathophysiological conditions.

The levels of NADH have been shown to increase during starvation and other pathophysiological conditions such as diabetes, alcoholic liver disease, and ischemia-reperfusion (42, 43). It has been shown that AO plays an important role in the alcohol-

induced liver injury due to its ability to generate ROS during the oxidation of acetaldehyde (44) or NADH (32). The level of NADH in normal rat liver is reported to be ~200–300 μM (Table 2). During ethanol metabolism the hepatic level of NADH has been reported to increase ~3-fold (45). Our EPR spin trapping and cytochrome c assay results show that the oxidation of NADH by AO produces $O_2^{\bullet-}$. It has also been shown that alcohol-induced ROS generated by AO can cause carcinogenic mutations and DNA damage leading to breast cancer (46). Hence, the production of ROS by the AO and NADH system can play a major role in alcohol induced liver disease and breast cancer.

In normal rat heart, the cellular level of NADH has been measured in the range of 40–80 μM (Table 2). During ischemia the level of NADH has been shown to increase ~10-fold (47). Also, the $O_2^{\bullet-}$ generation increases significantly under ischemic conditions (48). From our results, it is clear that the NADH oxidase activity of AO could be involved in the generation of $O_2^{\bullet-}$ during ischemia and may play an important role in oxidative damage.

A number of tissues and organs, such as micro- and macro-vasculature, peripheral nerves, kidney, heart, retina, and liver are affected in diabetes (49). Cytosolic NADH/NAD^+ ratio and level of ROS increase in diabetes (43). The increased production of NADH and ROS is important in the pathogenesis of diabetes and its complications (43, 49). Therefore, $O_2^{\bullet-}$ radical production through the oxidation of NADH by AO may play an important role in the pathophysiology of diabetes.

Overall, our studies demonstrate that NADH is an important substrate for AO as it has a high affinity for this enzyme and its oxidation by AO in the presence of produces large amounts of $O_2^{\bullet-}$. Although $O_2^{\bullet-}$ by itself is toxic, iron released from ferritin by AO (44) could catalyze the conversion of $O_2^{\bullet-}$ to the more toxic and highly reactive hydroxyl radical ($^{\bullet}OH$) or it could directly react with NO at diffusion controlled rate to produce peroxynitrite ($ONOO^-$), a powerful oxidant (50). Owing to its ubiquitous distribution along with its substrate NADH, AO would be predicted to function as an important cellular source of ROS under normal physiological conditions. With the increase in tissue NADH levels under various pathological conditions such as ischemia, alcohol induced liver diseases and diabetes, this ROS production would increase contributing to oxidative stress and free radical-mediated tissue injury/death.

Acknowledgments

The authors would like to thank Professor Russ Hille of the University of California, Riverside, for his help during the initial development of the purification protocol for AO. This work was supported by National Institute of Health grants HL63744, HL65608, and HL38324.

References

1. Hille R. The Mononuclear Molybdenum Enzymes. Chem Rev. 1996; 96:2757–2816. [PubMed: 11848841]
2. Hille R. Molybdenum-containing hydroxylases. Arch Biochem Biophys. 2005; 433:107–116. [PubMed: 15581570]
3. Stubley C, Stell JGP, Mathieson DW. The oxidation of azaheterocycles with mammalian liver aldehyde oxidase. Xenobiotica. 1979; 9:475–484. [PubMed: 516790]
4. Beedham C, Critchley DJ, Rance DJ. Substrate specificity of human liver aldehyde oxidase toward substituted quinazolines and phthalazines: a comparison with hepatic enzyme from guinea pig, rabbit, and baboon. Arch Biochem Biophys. 1995; 319:481–490. [PubMed: 7786031]
5. Kitamura S, Sugihara K, Ohta S. Drug-metabolizing ability of molybdenum hydroxylases. Drug Metab Pharmacokinet. 2006; 21:83–98. [PubMed: 16702728]

6. Ueda O, Sugihara K, Ohta S, Kitamura S. Involvement of molybdenum hydroxylases in reductive metabolism of nitro polycyclic aromatic hydrocarbons in mammalian skin. Drug Metab Dispos. 2005; 33:1312–1318. [PubMed: 15932950]
7. Calzi ML, Raviolo C, Ghibaudi E, de Gioia L, Salmona M, Cazzaniga G, Kurosaki M, Terao M, Garattini E. Purification, cDNA cloning, and tissue distribution of bovine liver aldehyde oxidase. J Biol Chem. 1995; 270:31037–31045. [PubMed: 8537361]
8. Kurosaki M, Demontis S, Barzago MM, Garattini E, Terao M. Molecular cloning of the cDNA coding for mouse aldehyde oxidase: tissue distribution and regulation in vivo by testosterone. Biochem J. 1999; 341(Pt 1):71–80. [PubMed: 10377246]
9. Kooij A, Schijns M, Frederiks WM, Van Noorden CJ, James J. Distribution of xanthine oxidoreductase activity in human tissues--a histochemical and biochemical study. Virchows Arch B Cell Pathol Incl Mol Pathol. 1992; 63:17–23. [PubMed: 1362018]
10. Kurosaki M, Li Calzi M, Scanziani E, Garattini E, Terao M. Tissue- and cell-specific expression of mouse xanthine oxidoreductase gene *in vivo*: regulation by bacterial lipopolysaccharide. Biochem J. 1995; 306(Pt 1):225–234. [PubMed: 7864814]
11. Linder N, Rapola J, Raivio KO. Cellular expression of xanthine oxidoreductase protein in normal human tissues. Lab Invest. 1999; 79:967–974. [PubMed: 10462034]
12. Engerson TD, McKelvey TG, Rhyne DB, Boggio EB, Snyder SJ, Jones HP. Conversion of xanthine dehydrogenase to oxidase in ischemic rat tissues. J Clin Invest. 1987; 79:1564–1570. [PubMed: 3294898]
13. Parks DA, Williams TK, Beckman JS. Conversion of xanthine dehydrogenase to oxidase in ischemic rat intestine: a reevaluation. Am J Physiol. 1988; 254:G768–G774. [PubMed: 3163236]
14. Nishino T, Okamoto K, Kawaguchi Y, Hori H, Matsumura T, Eger BT, Pai EF, Nishino T. Mechanism of the conversion of xanthine dehydrogenase to xanthine oxidase: identification of the two cysteine disulfide bonds and crystal structure of a non-convertible rat liver xanthine dehydrogenase mutant. J Biol Chem. 2005; 280:24888–24894. [PubMed: 15878860]
15. Nishino T, Nishino T. The conversion from the dehydrogenase type to the oxidase type of rat liver xanthine dehydrogenase by modification of cysteine residues with fluorodinitrobenzene. J Biol Chem. 1997; 272:29859–29864. [PubMed: 9368059]
16. Nishino T, Nishino T, Schopfer LM, Massey V. Reactivity of chicken liver xanthine dehydrogenase containing modified flavins. J Biol Chem. 1989; 264:6075–6085. [PubMed: 2539367]
17. McCord JM. Oxygen-derived free radicals in postischemic tissue injury. New Engl J Med. 1985; 312:159–163. [PubMed: 2981404]
18. Berry CE, Hare JM. Xanthine oxidoreductase and cardiovascular disease: molecular mechanisms and pathophysiological implications. J Physiol. 2004; 555:589–606. [PubMed: 14694147]
19. Kundu TK, Hille R, Velayutham M, Zweier JL. Characterization of superoxide production from aldehyde oxidase: an important source of oxidants in biological tissues. Arch Biochem Biophys. 2007; 460:113–121. [PubMed: 17353002]
20. Li H, Cui H, Kundu TK, Alzawahra W, Zweier JL. Nitric oxide production from nitrite occurs primarily in tissues not in the blood: critical role of xanthine oxidase and aldehyde oxidase. J Biol Chem. 2008; 283:17855–17863. [PubMed: 18424432]
21. Li H, Kundu TK, Zweier JL. Characterization of the magnitude and mechanism of aldehyde oxidase-mediated nitric oxide production from nitrite. J Biol Chem. 2009; 284:33850–33858. [PubMed: 19801639]
22. Kurth J, Kubiciel A. Method for the photometric determination of aldehyde oxidase activity. Biomed Biochim Acta. 1984; 43:1223–1226. [PubMed: 6532455]
23. Krenitsky TA, Spector T, Hall WW. Xanthine oxidase from human liver: purification and characterization. Arch Biochem Biophys. 1986; 247:108–119. [PubMed: 3010873]
24. Bradford MM. A rapid and sensitive method for the quantitation of microgram quantities of protein utilizing the principle of protein-dye binding. Anal Biochem. 1976; 72:248–254. [PubMed: 942051]

25. Sankarapandi S, Zweier JL. Bicarbonate is required for the peroxidase function of Cu, Zn-superoxide dismutase at physiological pH. J Biol Chem. 1999; 274:1226–1232. [PubMed: 9880490]
26. Fréjaville C, Karoui H, Tuccio B, Le Moigne F, Culcasi M, Pietri S, Lauricella R, Tordo P. 5-(Diethoxyphosphoryl)-5-methyl-1-pyrroline *N*-oxide: a new efficient phosphorylated nitrone for the *in vitro* and *in vivo* spin trapping of oxygen-centered radicals. J Med Chem. 1995; 38:258–265. [PubMed: 7830268]
27. Roubaud V, Sankarapandi S, Kuppusamy P, Tordo P, Zweier JL. Quantitative measurement of superoxide generation and oxygen consumption from leukocytes using electron paramagnetic resonance spectroscopy. Anal Biochem. 1998; 257:210–217. [PubMed: 9514781]
28. Cardounel AJ, Xia Y, Zweier JL. Endogenous methylarginines modulate superoxide as well as nitric oxide generation from neuronal nitric-oxide synthase: differences in the effects of monomethyl- and dimethylarginines in the presence and absence of tetrahydrobiopterin. J Biol Chem. 2005; 280:7540–7549. [PubMed: 15574418]
29. Massey V. The microestimation of succinate and the extinction coefficient of cytochrome c. Biochim Biophys Acta. 1959; 34:255–256. [PubMed: 14422133]
30. Nakamura M, Kurebayashi H, Yamazaki I. One-electron and two-electron reductions of acceptors by xanthine oxidase and xanthine dehydrogenase. J Biochem. 1978; 83:9–17. [PubMed: 24048]
31. Stell JGP, Warne AJ, Lee-Woolley C. Purification of rabbit liver aldehyde oxidase by affinity chromatography on benzamidine sepharose 6B. J Chromatogr. 1989; 475:363–372. [PubMed: 2777961]
32. Mira L, Maia L, Barreira L, Manso CF. Evidence for free radical generation due to NADH oxidation by aldehyde oxidase during ethanol metabolism. Arch Biochem Biophys. 1995; 318:53–58. [PubMed: 7726572]
33. Barr JT, Jones JP. Inhibition of human liver aldehyde oxidase: implications for potential drug-drug interactions. Drug Metab Dispos. 2011; 39:2381–2386. [PubMed: 21940905]
34. Obach RS. Potent inhibition of human liver aldehyde oxidase by raloxifene. Drug Metab Dispos. 2004; 32:89–97. [PubMed: 14709625]
35. Robertson IGC, Gamage RSKA. Methadone: a potent inhibitor of rat liver aldehyde oxidase. Biochem Pharmacol. 1994; 47:584–587. [PubMed: 8117328]
36. Beedham, C. Molybdenum Hydroxylases. In: Ioannides, C., editor. Enzyme Systems that Metabolise Drugs and Other Xenobiotics. John Wiley & Sons Ltd; UK: 2002. p. 147-187.
37. Pryde DC, Dalvie D, Hu Q, Jones P, Obach RS, Tran TD. Aldehyde oxidase: an enzyme of emerging importance in drug discovery. J Med Chem. 2010; 53:8441–8460. [PubMed: 20853847]
38. Rodrigues AD. Comparison of levels of aldehyde oxidase with cytochrome P450 activities in human liver *in vitro*. Biochem Pharmacol. 1994; 48:197–200. [PubMed: 8043023]
39. Sanders SA, Eisenthal R, Harrison R. NADH oxidase activity of human xanthine oxidoreductase--generation of superoxide anion. Eur J Biochem. 1997; 245:541–548. [PubMed: 9182988]
40. Maia L, Duarte RO, Ponces-Freire A, Moura JJ, Mira L. NADH oxidase activity of rat and human liver xanthine oxidoreductase: potential role in superoxide production. J Biol Inorg Chem. 2007; 12:777–787. [PubMed: 17440754]
41. Nakamura M. Allopurinol-insensitive oxygen radical formation by milk xanthine oxidase systems. J Biochem. 1991; 110:450–456. [PubMed: 1663114]
42. Ceconi C, Cargnoni A, Francolini G, Parinello G, Ferrari R. Heart rate reduction with ivabradine improves energy metabolism and mechanical function of isolated ischaemic rabbit heart. Cardiovasc Res. 2009; 84:72–82. [PubMed: 19477966]
43. Ido Y. Pyridine nucleotide redox abnormalities in diabetes. Antioxid Redox Signal. 2007; 9:931–942. [PubMed: 17508915]
44. Shaw S, Jayatilleke E. The role of cellular oxidases and catalytic iron in the pathogenesis of ethanol-induced liver injury. Life Sci. 1992; 50:2045–2052. [PubMed: 1608288]
45. Kato S, Kawase T, Alderman J, Inatomi N, Lieber CS. Role of xanthine oxidase in ethanol-induced lipid peroxidation in rats. Gastroenterology. 1990; 98:203–210. [PubMed: 2293579]
46. Wright RM, McManaman JL, Repine JE. Alcohol-induced breast cancer: a proposed mechanism. Free Radic Biol Med. 1999; 26:348–354. [PubMed: 9895226]

47. Kobayashi K, Neely JR. Effects of ischemia and reperfusion on pyruvate dehydrogenase activity in isolated rat hearts. J Mol Cell Cardiol. 1983; 15:359–367. [PubMed: 6876185]
48. Zweier JL, Talukder MA. The role of oxidants and free radicals in reperfusion injury. Cardiovasc Res. 2006; 70:181–190. [PubMed: 16580655]
49. Sivitz WI, Yorek MA. Mitochondrial dysfunction in diabetes: from molecular mechanisms to functional significance and therapeutic opportunities. Antioxid Redox Signal. 2010; 12:537–577. [PubMed: 19650713]
50. Goldstein S, Czapski G. The reaction of $NO^{\bullet}$ with $O_2^{\bullet-}$ and $HO_2^{\bullet}$: a pulse radiolysis study. Free Radic Biol Med. 1995; 19:505–510. [PubMed: 7590401]
51. Suleiman SA, Stevens JB. Purification of xanthine dehydrogenase from rat liver: a rapid procedure with high enzyme yields. Arch Biochem Biophys. 1987; 258:219–225. [PubMed: 3478001]
52. Harrison MF. Composition of the liver cell. Proc R Soc Lond B Biol Sci. 1953; 141:203–216. [PubMed: 13055860]
53. Xia Y, Zweier JL. Substrate control of free radical generation from xanthine oxidase in the postischemic heart. J Biol Chem. 1995; 270:18797–18803. [PubMed: 7642530]
54. Henriksen EJ, Munoz KA, Aannestad AT, Tischler ME. Cardiac protein content and synthesis in vivo after voluntary running or head-down suspension. J Appl Physiol. 1994; 76:2814–2819. [PubMed: 7928915]
55. Williamson, JR.; Steenbergen, C.; Rich, T.; Deleeuw, G.; Barlow, C.; Chance, B. The nature of ischemic injury in cardiac tissue. In: Lefer, AM.; Kelliher, GH.; Rovetto, MJ., editors. Pathophysiology and Therapeutics of Myocardial Ischemia. Spectrum Publications, Inc; New York: 1977. p. 193-225.
56. Lowry OH, Passonneau JV, Schulz DW, Rock MK. The measurement of pyridine nucleotides by enzymatic cycling. J Biol Chem. 1961; 236:2746–2755. [PubMed: 14466981]
57. Jacobson KB, Kaplan NO. Pyridine coenzymes of subcellular tissue fractions. J Biol Chem. 1957; 226:603–613. [PubMed: 13438846]

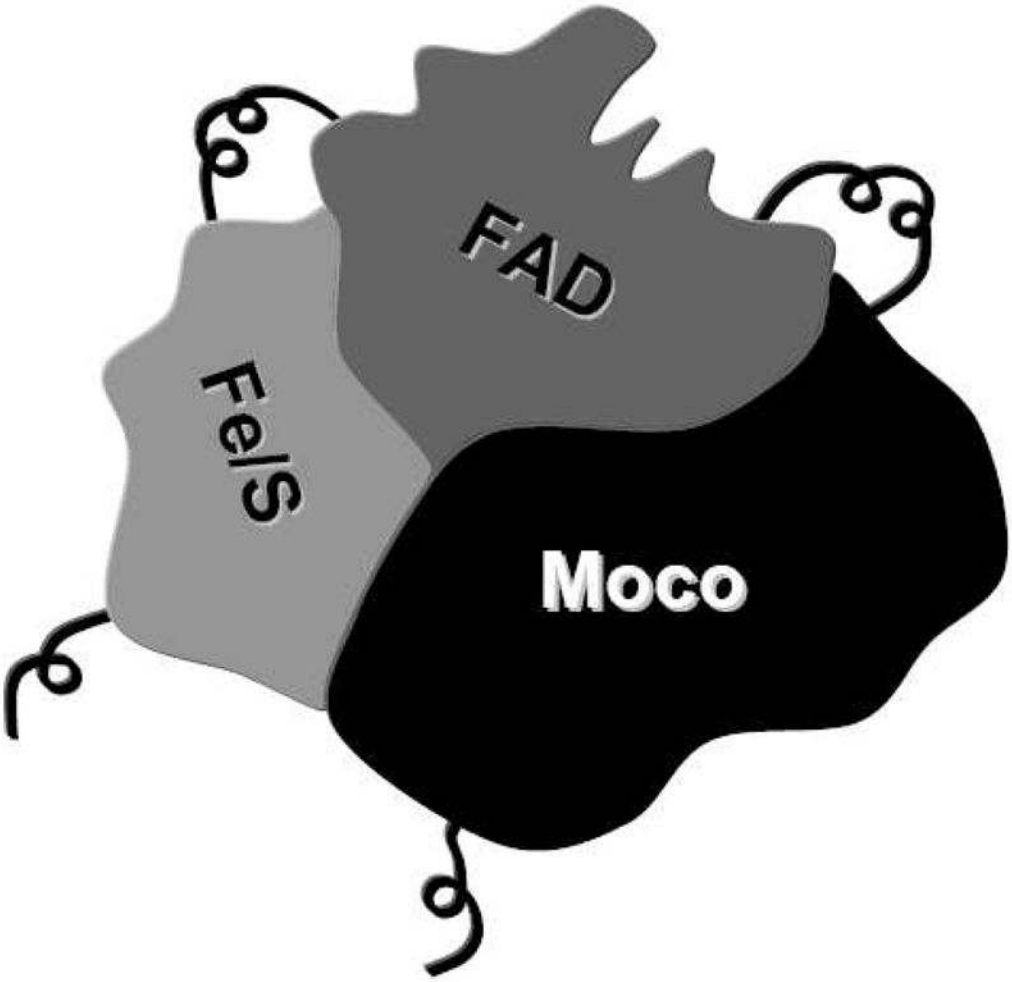

Figure 1. Domains of liver aldehyde oxidase and xanthine oxidoreductase

Each subunit has a typical tripartite structure consisting of an N-terminal domain (~20 kDa) containing two spectroscopically distinct 2Fe-2S redox centers, a central FAD binding domain (~40 kDa) and a large C-terminal domain (~85 kDa) comprising the substrate-binding pocket and the molybdenum cofactor (Moco) binding site. Each iron-sulfur center functions as a one-electron acceptor whereas FAD and molybdenum centers function as two-electron acceptors. Both iron-sulfur centers act as electron-sinks maintaining molybdenum oxidized and FAD reduced during enzyme turnover.

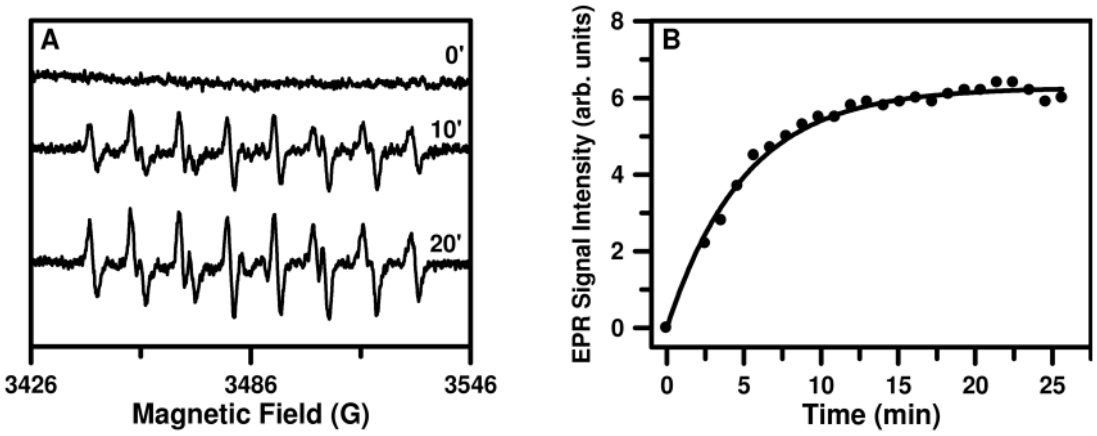

Figure 2. Time-dependent $O_2^{\bullet -}$ generation during the reaction of NADH with AO measured with the spin trap DEPMPO

The reaction mixture consists of 120 μM NADH, 400 μM DTPA, 20 mM DEPMPO, and 25 mU/mL AO in 50 mM air-saturated phosphate buffer (pH 7.8) at 21 °C: (A) EPR spectra of $\mathrm{DEPMPO}/O_2^{\bullet -}$ radical adducts recorded as a function of time; (B) Graph of signal intensities of the 4th peak (from low field) of the EPR spectra, 1-scan per min, recorded continuously for 25 min. Instrumental conditions are as described in the "Materials and Methods" section.

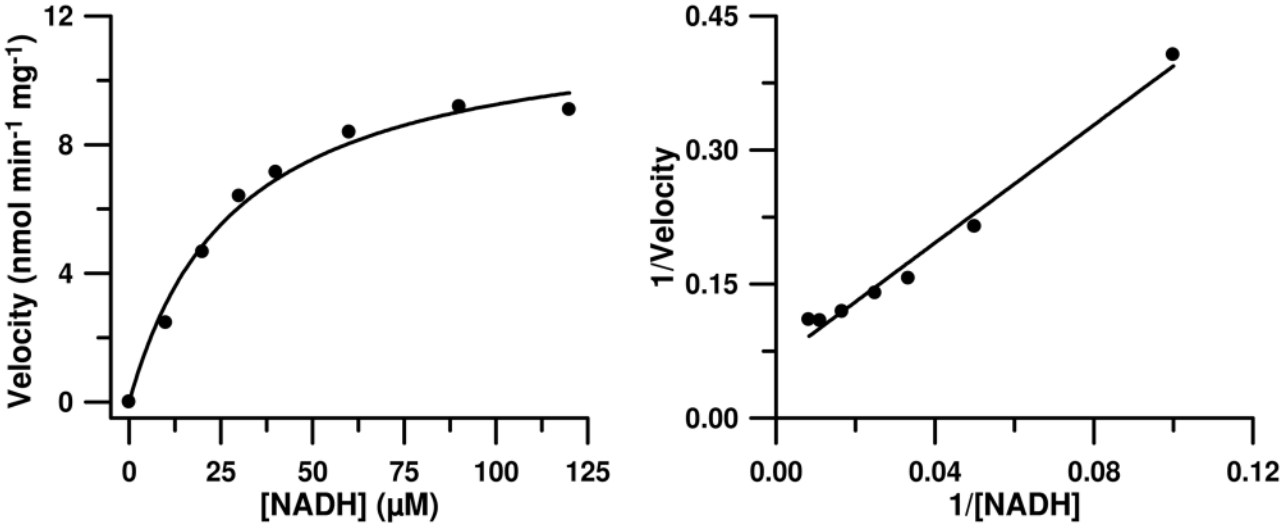

Figure 3. NADH oxidation by rat liver AO

Reactions were performed in the presence of 100 U/mL catalase and 250 U/mL SOD1 in air-saturated 50 mM phosphate buffer (pH 7.8) containing 0.1 mM EDTA at 21 °C. In each experiment the concentration of NADH was varied with a fixed amount (20 mU/mL) of AO. The rates of NADH oxidation were determined by monitoring the change in absorbance at 340 nm in the presence of various concentrations of NADH. Data were fitted to the Michaelis-Menten equation (*left*) with K_m and V_{max} values as 29.1 ± 4.5 μM and 11.9 ± 0.7 nmol min^{-1} mg^{-1} of protein, respectively. The Lineweaver-Burk plot is shown on the *right*.

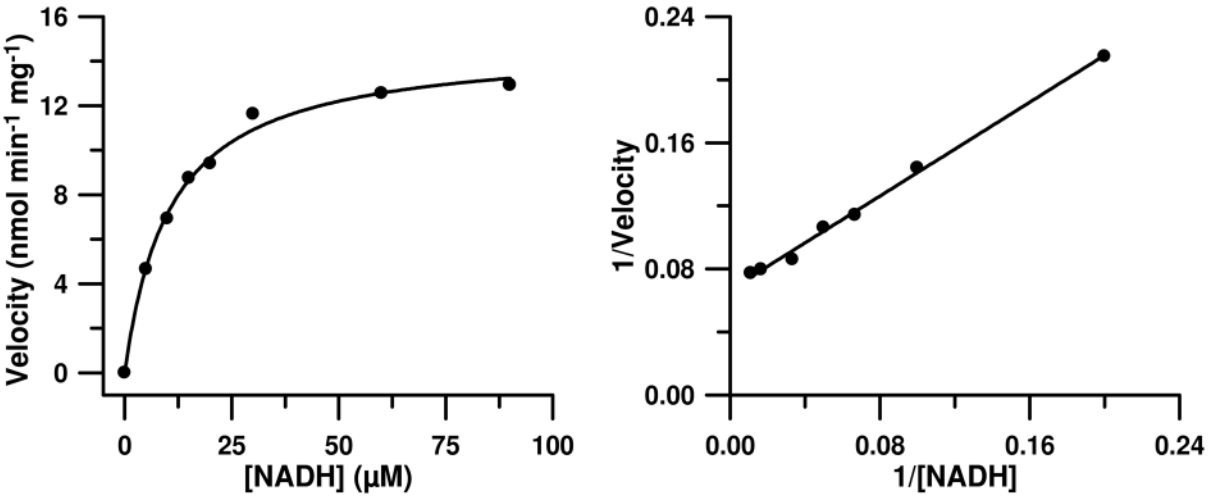

Figure 4. Production of $O_2^{\bullet-}$ by rat liver AO using NADH as a substrate

Reactions were performed in air-saturated 50 mM phosphate buffer (pH 7.8) containing 0.1 mM EDTA at 21 °C. The rates of $O_2^{\bullet-}$ formation were determined by monitoring the SOD1-inhibitable reduction of 100 μM cytochrome c at 550 nm in the presence of 100 U/mL catalase, 29 mU/mL AO, and various concentrations of NADH. Actual rates as calculated by subtracting the control rates from the original rates were used to calculate the initial velocities. Data were fitted to the Michaelis-Menten equation (*left*) with K_m and V_{max} values as 10.7 ± 0.9 μM and 14.8 ± 0.4 nmol min^{-1} mg^{-1} of protein, respectively. The Lineweaver-Burk plot is shown on the *right*.

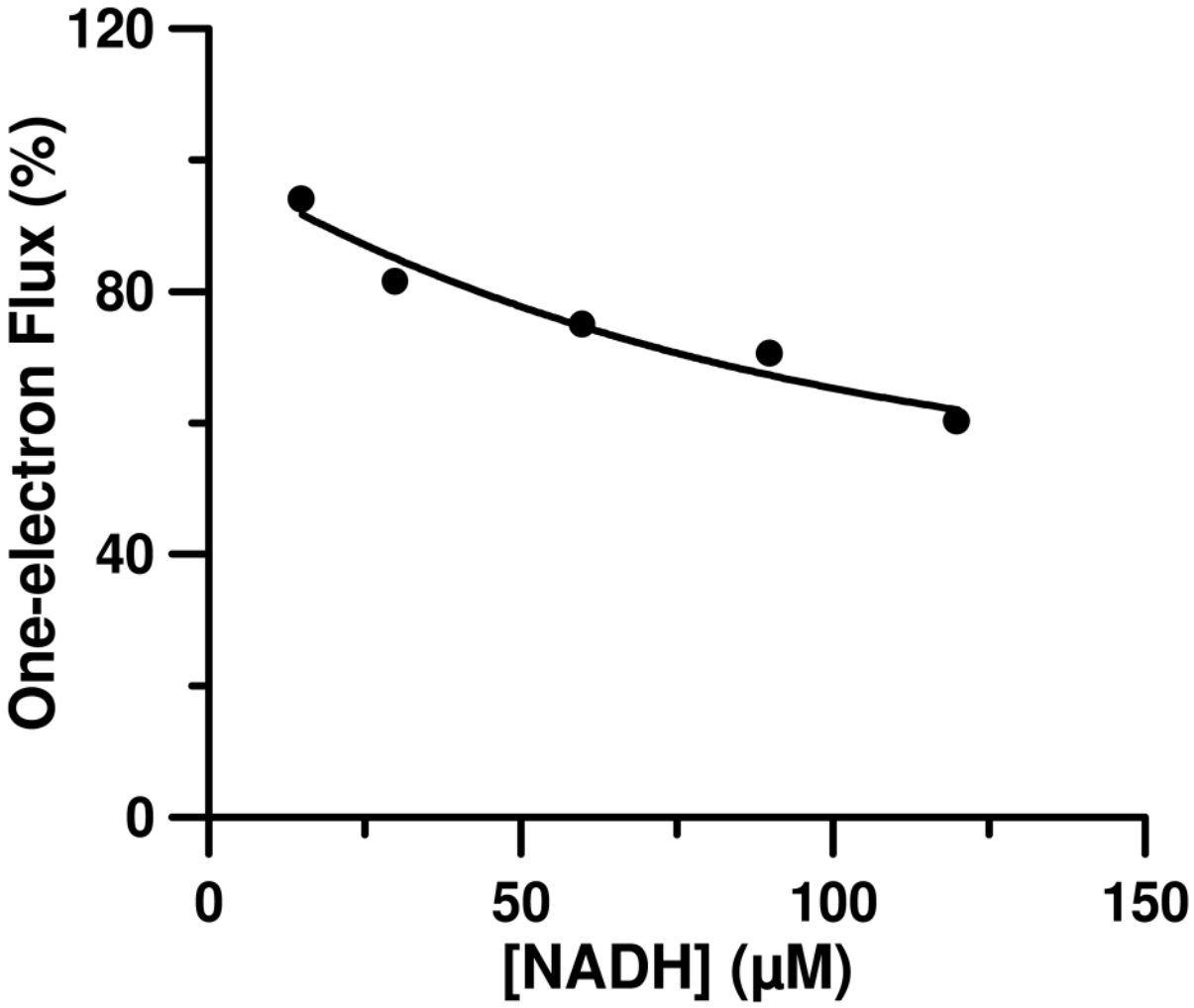

Figure 5. Percentage of one-electron flux as a function of the concentration of NADH during the oxidation of NADH by AO

The one-electron flux was calculated from the ratio of the rate of $O_2^{\bullet -}$-mediated reduction of ferricytochrome c to the rate of NADH oxidation as described in the text (Eq. 2).

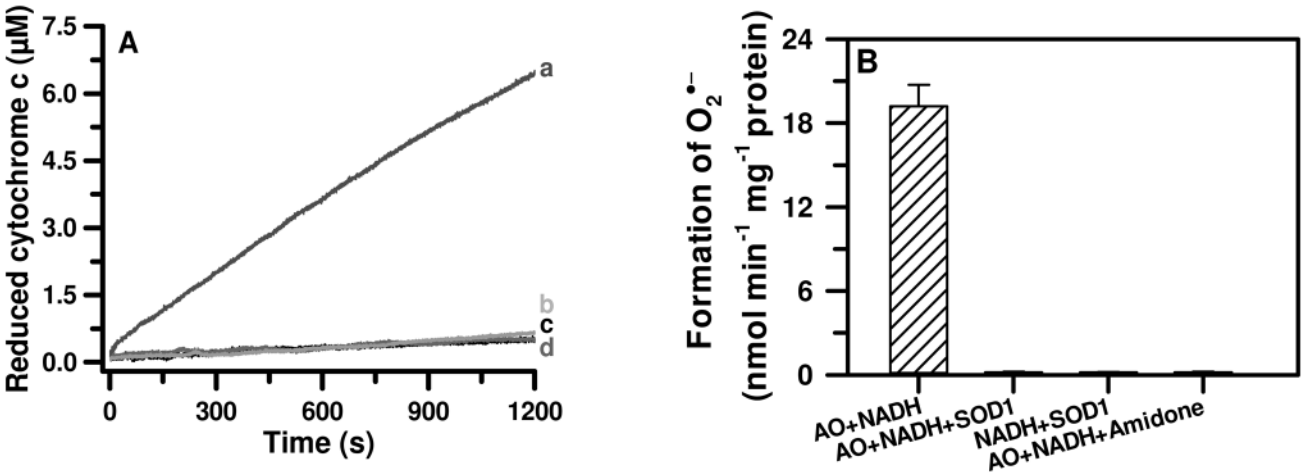

Figure 6. Cytochrome c assay for the generation of $O_2^{\bullet-}$ during the oxidation of NADH by AO

(A) The reaction mixture, in a final volume of 1 mL, contained 100 mM phosphate buffer (pH 7.8), 0.1 mM EDTA, 100 μM ferricytochrome c, 120 μM NADH, and 22 mU/mL AO. Reduction of ferricytochrome c by $O_2^{\bullet-}$ was monitored at 550 nm: **(a)** complete system; **(b)** same as **a** plus 200 U/mL SOD1; **(c)** same as **b** but without AO; **(d)** same as **a** plus 100 μM amidone; **(B)** Graph summarizing the inhibition of $O_2^{\bullet-}$ generation in repeat experiments for the various conditions described in **A**. The bars show mean values ± SE.

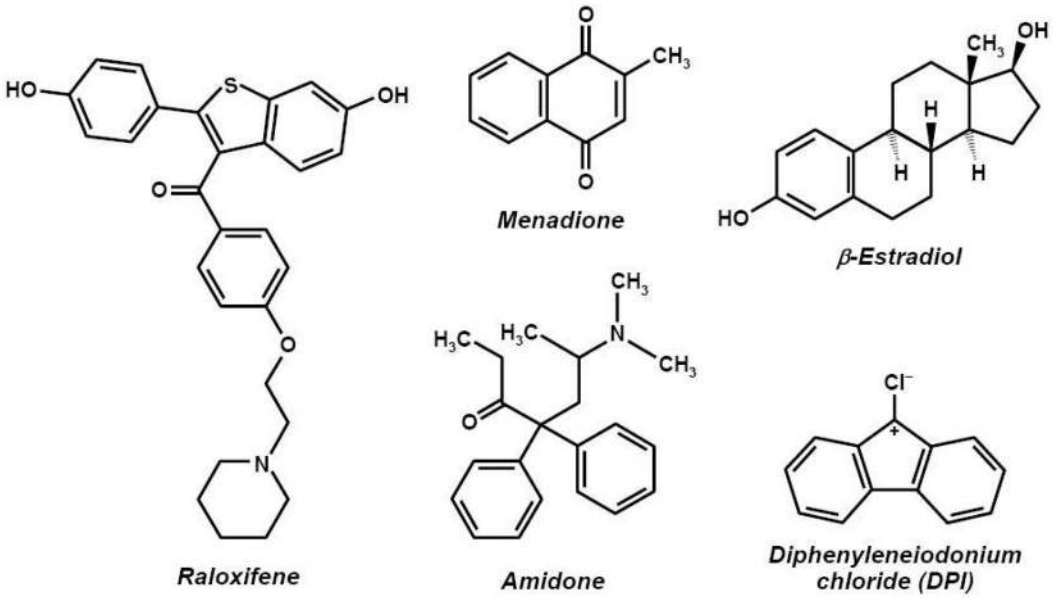

Figure 7. Chemical structures of various AO inhibitors used

Except diphenyleneiodonium which is a non-specific inhibitor of FAD containing enzymes, all other inhibitors have been reported as specific inhibitors of AO although each may have other functions as well.

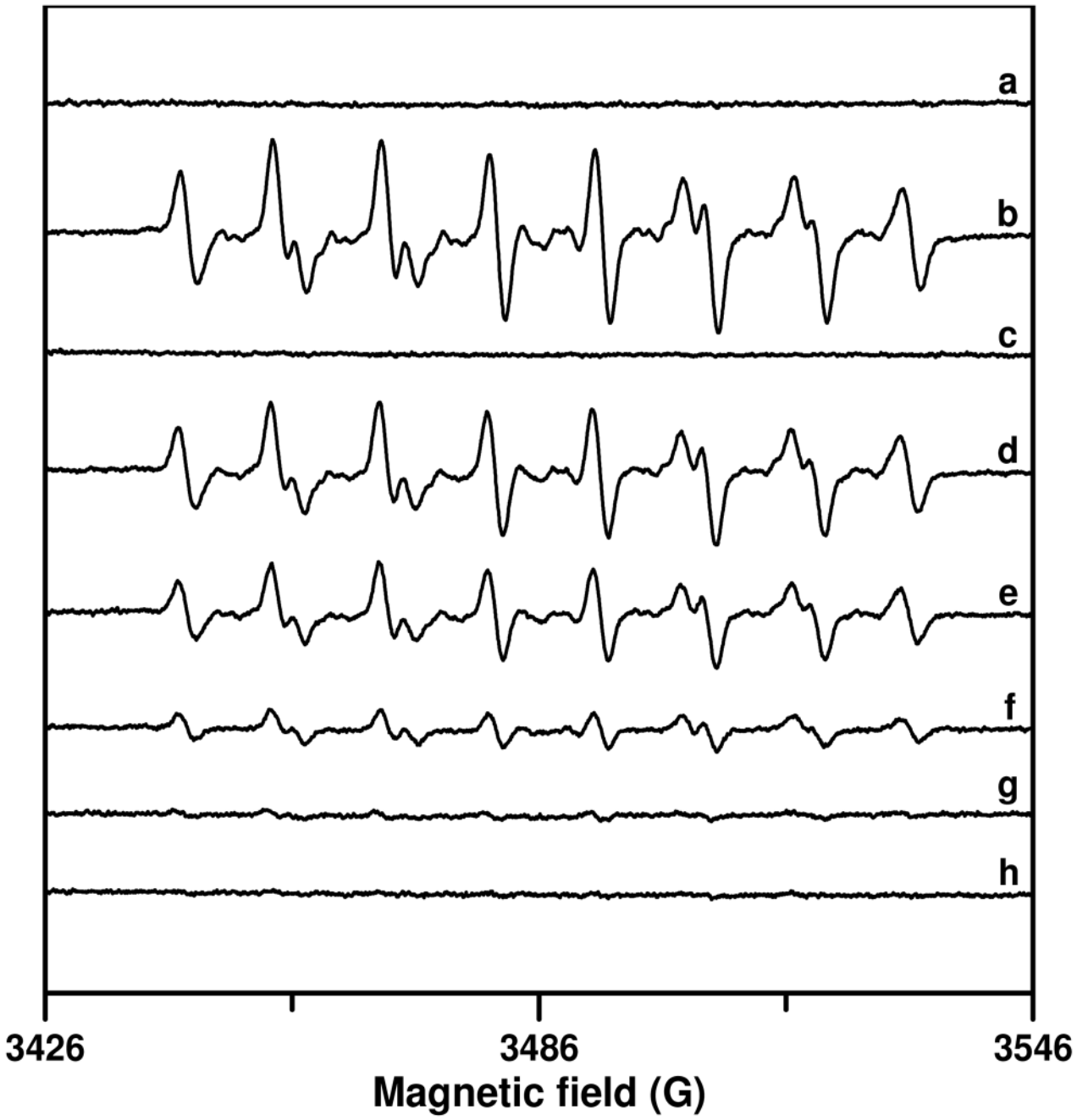

Figure 8. EPR spectra of DEPMPO-$O_2^{\bullet-}$ radical adducts recorded during the reaction of NADH with AO

The spectra were recorded after incubation of 110 μM NADH, 400 μM DTPA, 20 mM DEPMPO, and 25 mU/mL AO for 80 sec at 21 °C in 50 mM phosphate buffer (pH 7.8): **(a)** complete system, but without AO; **(b)** complete system; **(c)** same as **b** but in the presence of 250 U/mL SOD1; **(d)** same as **b** but in the presence of 150 μM β-estradiol; **(e)** same as **b** but in the presence of 150 μM raloxifene; **(f)** same as **b** but in the presence of 150 μM menadione; **(g)** same as **b** but in the presence of 100 μM amidone; **(h)** same as **b** but in the presence of 150 μM DPI. Instrumental conditions are as described in the "Materials and Methods" section.

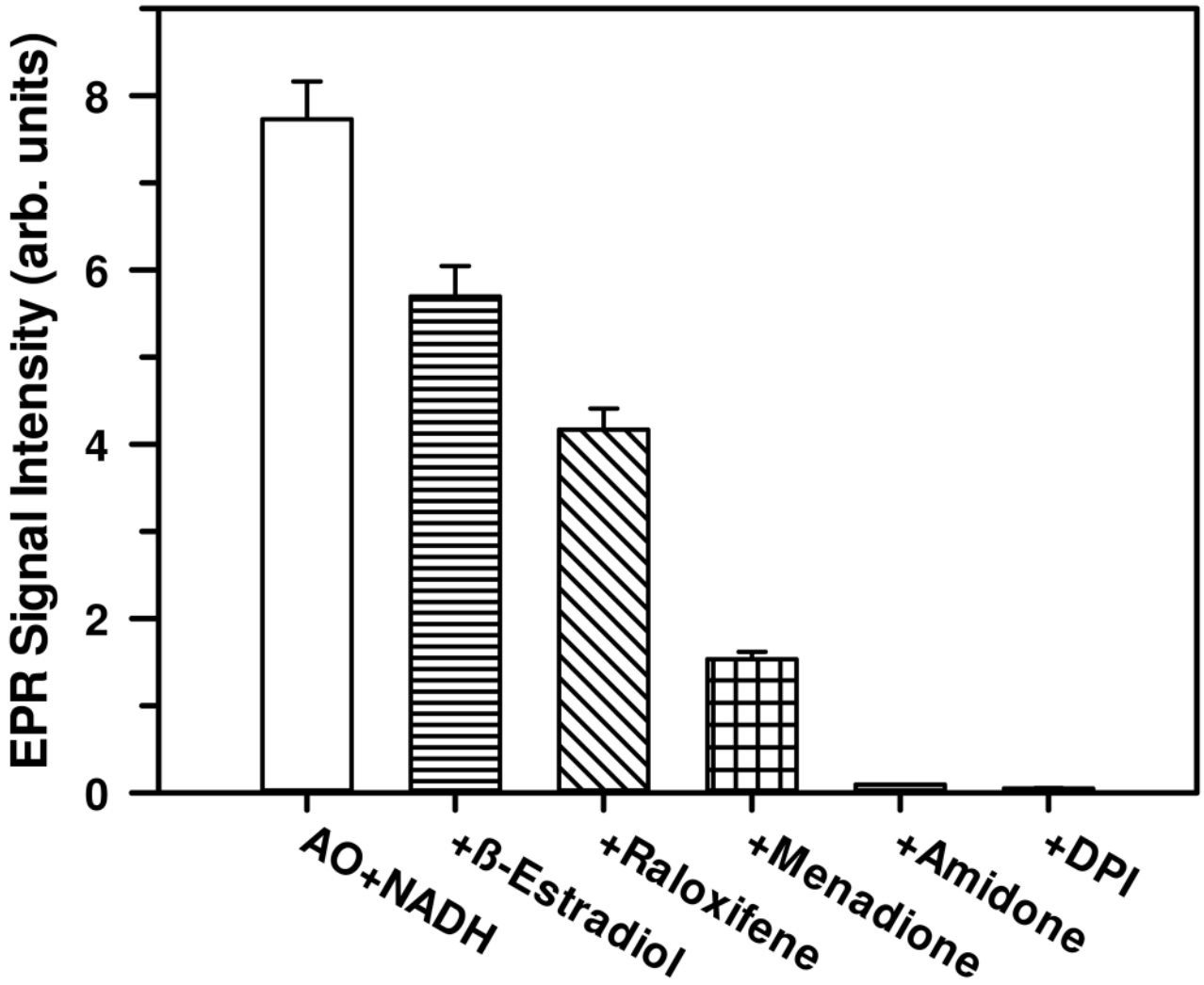

Figure 9. Effect of various inhibitors of AO on the reaction of NADH with AO in presence of DEPMPO

From a series of repeat experiments, the intensities of 4th peak (from low field) of EPR spectra as seen in figure 8 were plotted for each of the inhibitors used with mean values ± SE. At a final concentration of 150 μM β-estradiol, raloxifene, menadione, and DPI caused 26.0±2.7, 46.1±1.8, 80.5±1.4, and 99.9±0.1% inhibition, respectively; at a final concentration of 100 μM amidone caused 99.3±0.1% inhibition. All the inhibitors significantly decreased $O_2^{\bullet -}$ generation compared to the untreated control, $P < 0.022$ for β-estradiol and $P < 0.001$ for all the others.

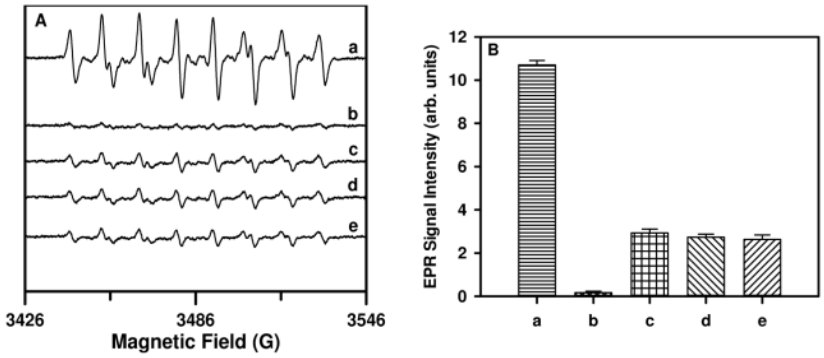

Figure 10. Effect of amidone on the generation of $O_2^{\bullet-}$ by AO and XO using NADH as a substrate

(A) EPR spectra of $\mathrm{DEPMPO}/O_2^{\bullet-}$ radical adducts generated by AO or XO and NADH. The reaction mixture consisting of 110 μM NADH, 400 μM DTPA, 20 mM DEPMPO, and either 25 mU/mL of AO or XO was incubated for 65 sec at 21 °C in 50 mM phosphate buffer (pH 7.8): **(a)** complete system with AO; **(b)** same as **a** but in the presence of 100 μM amidone; **(c)** complete system with XO; **(d)** same as **c** but in the presence of 100 μM amidone; **(e)** same as **c** but in the presence of 1 mM amidone; **(B)** Intensities of the 4th peak (from low field) of the EPR spectra from a series of repeat experiments as depicted in **A** either in the absence or presence of amidone. The bars show mean values ± SE. While amidone completely inhibits the $O_2^{\bullet-}$ formation by AO/NADH system, it does not affect the $O_2^{\bullet-}$ generation by XO/NADH.

Table 1

Comparison of the levels of AO and XOR in rat heart and liver.[1]

Enzyme sources	XOR					AO	
	Sp. activity (nmol min^{-1} g^{-1} protein)			Total protein (mg/g wet wt. of tissue)	[XOR] (nM)	Sp. activity (nmol min^{-1} g^{-1} protein)[2]	[AO] (nM)
	XDH	XO	Total XOR				
Rat liver	2148[51]	352[51]	2500[51]	180[52]	1160	3900	1208
Rat heart	130[53]	8.4[53]	138[53]	155[54]	50	209	51

[1]Concentrations of AO and XOR were calculated assuming cell water contents for heart and liver of 0.580 and 0.527 mL/g wet wt. of tissue, respectively.

[2]This work; activities of AO were calculated using *p*-DMAC as substrates, respectively.

Table 2

Tissue levels of NAD^+, NADH, and their ratios in rat liver and heart.[3]

Tissue sources	Control			Ischemia		
	[NAD^+] (μM)	[NADH] (μM)	[NAD^+]/[NADH]	[NAD^+] (μM)	[NADH] (μM)	[NAD^+]/[NADH]
Perfused rat heart[55]	1385	83	16.7	1082	443	2.4
Perfused rat heart[47]	1075	39	27.7	732	404	1.8
Rat liver[56]	891	358	2.5	–	–	–
Rat liver[57]	943	210	4.5	–	–	–

[3]The concentrations of pyridine nucleotides from literatures reports are shown. Total tissue water content in the liver and heart are considered as 0.705 and 0.789 mL/g wet weight of tissue, respectively.